

Combined effects of crab dispersion and momentum dispersion in colliders with local crab crossing scheme

Derong Xu^{*} and Yun Luo

Brookhaven National Laboratory, Upton, New York 11973, USA

Yue Hao

Michigan State University, East Lansing, Michigan 48824, USA



(Received 6 May 2022; accepted 18 July 2022; published 28 July 2022)

In this paper, we present the effects of linear transverse-longitudinal coupling on beam size at the interaction point (IP) of a collider with a local crab crossing scheme, when time-dependent transverse deflection (crab kicks) and dispersive orbit intertwine near IP. The analytic propagation formula and the closed orbit form of the crab dispersion and momentum dispersion are derived. The nonzero momentum dispersion at crab cavities and the nonideal phase from crab cavities to IP are detailed with the derived propagation formula to predict the beam size distortion at IP with or without the beam-beam interaction. The linear results are compared with nonlinear simulation using the weak-strong beam-beam code.

DOI: [10.1103/PhysRevAccelBeams.25.071002](https://doi.org/10.1103/PhysRevAccelBeams.25.071002)

I. INTRODUCTION

A large crossing angle in the interaction region (IR) is necessary for the fast separation of two colliding beams in ring-ring type colliders to achieve high collision rates, IR background minimization, and overall detector component and IR magnet arrangements. Crab cavities, first proposed for linear colliders [1], can compensate for the geometrical luminosity loss induced by crossing angle. This idea was later expanded to include circular colliders [2].

The crab cavity generates a transverse kick, depending on the longitudinal coordinate z of a particle. Due to symplecticity, the particle always receives an energy kick from the crab cavity as a function of transverse offset x simultaneously, as shown in Eq. (1).

$$\begin{aligned}\Delta p_x &= -\lambda \sin(k_c z + \phi_c)/k_c \\ \Delta \delta &= -\lambda \cos(k_c z + \phi_c)x,\end{aligned}\quad (1)$$

where Δp_x and $\Delta \delta$ are horizontal and momentum kick from the crab cavity, λ is the kick strength normalized by the momentum of the reference particle, k_c and ϕ_c are the wave number and synchronous phase of the crab cavity, respectively.

In the crab crossing scheme, both colliding beams are tilted by half crossing angle in the x - z plane to restore

the head-on collision. There are two configurations to accomplish this: global and local schemes. In a global scheme, the crab cavity is placed at a particular location and the horizontal and longitudinal dynamics is coupled all over the ring. In a local scheme, a pair of crab cavities are installed at both sides of the IP. The upstream crab cavity tilts the beam in the x - z plane, and the downstream crab cavity rotates the beam back. In the rest of the rings, both planes stay unaffected.

The global scheme was first successfully implemented at the KEKB B-Factory (High Energy Accelerator Research Organisation) [3], where a world record luminosity of $2.1 \times 10^{34} \text{ cm}^{-2} \text{ s}^{-1}$ was obtained. The local scheme was also demonstrated for the hadron beam in CERN's Super Proton Synchrotron (SPS) [4]. The Electron-Ion Collider (EIC) also adopts the local scheme to achieve the desired luminosity ($1 \times 10^{34} \text{ cm}^{-2} \text{ s}^{-1}$) [5]. A schematic of the local crabbing compensation scheme is shown in Fig. 1 where two sets of crab cavities are placed on both sides of IP for each ring.

The single crab cavity dynamics in the global crabbing scheme has been studied in detail. In the absence of longitudinal motion, the linear effect of crab cavities on the closed orbit is described by the concept of z -dependent dispersion [6], which is referred as the crab dispersion throughout this study. The linear transverse and longitudinal coupled motion due to crab cavities is analyzed through the transfer matrix in [7]. The synchro-betatron stop bands due to a single crab cavity are calculated in [8]. The impact on the luminosity or the dynamical aperture is discussed in [9,10].

However, the crab cavity voltage in the global scheme depends on the linear beam optics which is distorted by the beam-beam interaction. The crab dispersion all over the

*dxu@bnl.gov

Published by the American Physical Society under the terms of the *Creative Commons Attribution 4.0 International license*. Further distribution of this work must maintain attribution to the author(s) and the published article's title, journal citation, and DOI.

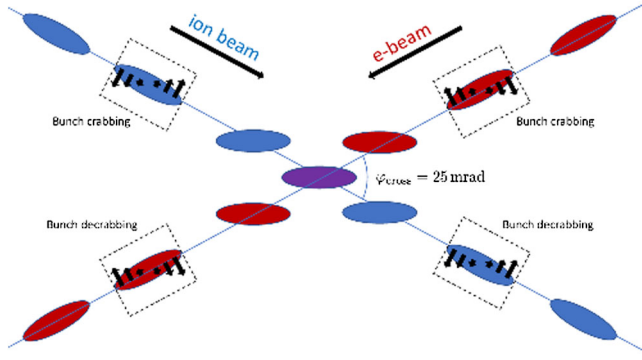


FIG. 1. EIC local crabbing compensation scheme.

ring excites various synchro-betatron resonances. From KEKB operation experiences, the global scheme may be sensitive to the chromatic coupling and machine errors [10]. These can be avoided or mitigated in a local crabbing scheme as the crab dispersion is constrained within IR.

In the ideal local crabbing scheme, the two crab cavities, located at the location with the betatron phase advance of $\pm\pi/2$ from IP, create desired crab dispersion “bump” between them. The crab dispersion outside the crab cavity pair vanishes. Under this ideal assumption, the nonlinear z dependence from rf curvature and its impact on beam dynamics is described in [11].

On the other hand, nonideal crab-crossing setups also impact the dynamics of the colliding beams. The imperfections include the presence of dispersion at crab cavities which are first discussed in [12] and unmatched betatron phase advance between the crab cavity pair. They break the closure of the crab dispersion bump and may cause degradation of beam quality and luminosity. We present a theoretical treatment for the interplay of momentum and crab dispersion with these imperfections, then verify the predictions with the presence of the beam-beam effect in weak-strong simulations.

This paper is organized as follows: Section II extends the concept of crab dispersion and momentum dispersion to the 6D phase space. Section III applies the theory to explain the effects of nonzero momentum dispersion at crab cavities and nonideal phase advance from crab cavities to IP. Section IV shows the results of combining the momentum/crab dispersion effects with the beam-beam effect in a weak-strong simulation. The conclusion is given in Sec. V.

II. CRAB DISPERSION AND MOMENTUM DISPERSION

When the transverse coordinates x, p_x, y , and p_y are coupled with the longitudinal offset z as well as the relative momentum deviation δ , neither z nor δ is constant. In consequence, the regular momentum dispersion is no longer well defined. We can instead define it as follows:

Let \mathcal{M} be a canonical transformation

$$(x, p_x, y, p_y, z, \delta)^T = \mathcal{M}(\bar{x}, \bar{p}_x, \bar{y}, \bar{p}_y, \bar{z}, \bar{\delta})^T, \quad (2)$$

where the superscript “T” denotes the transformation of a vector or a matrix. In the new phase space of $\{\bar{x}, \bar{p}_x, \bar{y}, \bar{p}_y, \bar{z}, \bar{\delta}\}$, the longitudinal and transverse motion is decoupled. Then the momentum dispersion and the crab dispersion are defined as

$$\boldsymbol{\eta} \equiv \frac{\partial \mathbf{X}}{\partial \delta}, \quad \boldsymbol{\zeta} \equiv \frac{\partial \mathbf{X}}{\partial \bar{z}}, \quad (3)$$

where \mathbf{X} is the abbreviation of $(x, p_x, y, p_y)^T$. \bar{z} and $\bar{\delta}$ are connected by the longitudinal oscillation. As a result, the two kinds of dispersion are also interchangeable.

When the crab dispersion is not present, the transformation is well known [13]

$$\mathcal{M}_\eta = \begin{bmatrix} \mathbf{1}_{4 \times 4} & \mathbf{0}_{4 \times 1} & \boldsymbol{\eta} \\ -(\mathbf{J}\boldsymbol{\eta})^T & 1 & 0 \\ \mathbf{0}_{1 \times 4} & 0 & 1 \end{bmatrix}, \quad (4)$$

where J is the 4-by-4 symplectic form matrix

$$J = \begin{bmatrix} 0 & 1 & 0 & 0 \\ -1 & 0 & 0 & 0 \\ 0 & 0 & 0 & 1 \\ 0 & 0 & -1 & 0 \end{bmatrix}. \quad (5)$$

Similarly, the transformation of the crab dispersion is

$$\mathcal{M}_\zeta = \begin{bmatrix} \mathbf{1}_{4 \times 4} & \boldsymbol{\zeta} & \mathbf{0}_{4 \times 1} \\ \mathbf{0}_{1 \times 4} & 1 & 0 \\ (\mathbf{J}\boldsymbol{\zeta})^T & 0 & 1 \end{bmatrix}. \quad (6)$$

When both kinds of dispersion are present, we can make a succession of the two canonical transformations [Eqs. (4) and (6)],

$$\begin{aligned} \mathcal{M} &= \mathcal{M}_\zeta \mathcal{M}_\eta \\ &= \begin{bmatrix} \mathbf{1}_{4 \times 4} - \boldsymbol{\zeta}(\mathbf{J}\boldsymbol{\eta})^T & \boldsymbol{\zeta} & \boldsymbol{\eta} \\ -(\mathbf{J}\boldsymbol{\eta})^T & 1 & 0 \\ (\mathbf{J}\boldsymbol{\zeta})^T & 0 & 1 + (\mathbf{J}\boldsymbol{\zeta})^T \boldsymbol{\eta} \end{bmatrix}. \end{aligned} \quad (7)$$

Substituting it back into Eq. (2), it is straightforward to check that the transformation in Eq. (7) accommodates the definition in Eq. (3),

$$\mathbf{X} = M\bar{\mathbf{X}} + \boldsymbol{\zeta}\bar{z} + \boldsymbol{\eta}\bar{\delta}, \quad (8)$$

where M is the 4-by-4 block of \mathcal{M} .

The transformation $\mathcal{M}_\eta\mathcal{M}_\zeta$ also holds true for the definition in Eq. (3). However, $\mathcal{M}_\zeta\mathcal{M}_\eta$ is a better choice from the viewpoint of beam-beam study. From Hirata [14], the linear map for the Lorentz boost in the crab crossing scheme is

$$\mathcal{L} \approx \begin{bmatrix} 1 & 0 & 0 & 0 & \theta_c & 0 \\ 0 & 1 & 0 & 0 & 0 & 0 \\ 0 & 0 & 1 & 0 & 0 & 0 \\ 0 & 0 & 0 & 1 & 0 & 0 \\ 0 & 0 & 0 & 0 & 1 & 0 \\ 0 & -\theta_c & 0 & 0 & 0 & 1 \end{bmatrix}, \quad (9)$$

where θ_c is the half crossing angle, and the approximation $\theta_c \approx 0$ is used. The linear Lorentz boost \mathcal{L} is literally a crab transformation with $\zeta = (\theta_c, 0, 0, 0)^\top$. To provide an effective head-on collision, the crab dispersion and the momentum dispersion are found to be

$$\mathcal{L}\mathcal{M} = \mathbf{1}_{6 \times 6} \Rightarrow \zeta^* = (-\theta_c, 0, 0, 0)^\top, \quad \eta^* = \mathbf{0}_{4 \times 1}, \quad (10)$$

where the superscript symbol “*” denotes IP. The property $\mathcal{M}_\zeta(\zeta_1)\mathcal{M}_\zeta(\zeta_2) = \mathcal{M}_\zeta(\zeta_1 + \zeta_2)$ is used in Eq. (10).

The linear motion through a section can be expressed via the 6-by-6 transfer matrix \mathcal{R} . In the phase space of $\{\bar{x}, \bar{p}_x, \bar{y}, \bar{p}_y, \bar{z}, \bar{\delta}\}$, the transfer matrix will be

$$\bar{\mathcal{R}} = \mathcal{M}_2^{-1}\mathcal{R}\mathcal{M}_1 \quad \text{or} \quad \mathcal{M}_2\bar{\mathcal{R}} = \mathcal{R}\mathcal{M}_1, \quad (11)$$

where points 1 and 2 are the entrance and the exit of this section, respectively. According to the definition, the matrix $\bar{\mathcal{R}}$ is block diagonalized, i.e.,

$$\begin{aligned} \bar{r}_{i5} &= 0, & \bar{r}_{i6} &= 0, \\ \bar{r}_{5i} &= 0, & \bar{r}_{6i} &= 0, \end{aligned} \quad (12)$$

where $i = 1, 2, 3, 4$, and \bar{r}_{ij} are the matrix elements of $\bar{\mathcal{R}}$ at i th row, j th column.

There are eight free variables in \mathcal{M}_2 . In the meantime, the number of independent constraints in Eq. (12) is also 8. In principle, ζ_2 and η_2 are determined by Eqs. (11) and (12). The propagation of the crab dispersion and momentum dispersion can be resolved.

When the particle travels through a momentum dispersing section without any crab cavities or rf cavities, the 6-by-6 transfer matrix will be

$$\mathcal{R}_{\text{dis}} = \begin{bmatrix} R_d & \mathbf{0}_{4 \times 1} & \mathbf{D} \\ \mathbf{B}^\top & 1 & r_{56} \\ \mathbf{0}_{1 \times 4} & 0 & 1 \end{bmatrix}, \quad (13)$$

where R_d is the 4-by-4 block, and \mathbf{D} is the momentum dispersion generator. The symplectic condition requires

$$R_d^\top J R_d = J, \quad \mathbf{B}^\top = \mathbf{D}^\top J R_d. \quad (14)$$

The block diagonalized matrix $\bar{\mathcal{R}}_{\text{dis}}$ has a form of

$$\bar{\mathcal{R}}_{\text{dis}} = \begin{bmatrix} \bar{R}_d & \mathbf{0}_{4 \times 1} & \mathbf{0}_{4 \times 1} \\ \mathbf{0}_{1 \times 4} & \bar{r}_{55} & \bar{r}_{56} \\ \mathbf{0}_{1 \times 4} & 0 & \bar{r}_{66} \end{bmatrix}, \quad (15)$$

with the symplectic constraint

$$\bar{R}_d^\top J \bar{R}_d = J, \quad \bar{r}_{55}\bar{r}_{66} = 1. \quad (16)$$

Substituting Eqs. (7), (13), and (15) into Eq. (11), it follows that

$$\begin{aligned} \bar{r}_{55} &= 1 + \mathbf{B}^\top \zeta_1, & \zeta_2 &= R_d \zeta_1 / \bar{r}_{55}, \\ \bar{r}_{56} &= \mathbf{B}^\top \eta_1 + r_{56}[1 + (J\zeta_1)^\top \eta_1], \\ \eta_2 &= \bar{r}_{55}\{R_d \eta_1 + \mathbf{D}[1 + (J\zeta_1)^\top \eta_1]\} - \bar{r}_{56}R_d \zeta_1. \end{aligned} \quad (17)$$

When $\zeta_1 = \mathbf{0}_{4 \times 1}$, the propagation turns into

$$\zeta_2 = \mathbf{0}_{4 \times 1}, \quad \eta_2 = R_d \eta_1 + \mathbf{D}, \quad (18)$$

which is the same as the normal dispersion propagation.

When the particle passes by a cavity-like element, the linear transfer matrix is

$$\mathcal{R}_{\text{cav}} = \begin{bmatrix} R_c & \mathbf{C} & \mathbf{0}_{4 \times 1} \\ \mathbf{0}_{1 \times 4} & 1 & 0 \\ \mathbf{A}^\top & r_{65} & 1 \end{bmatrix}, \quad (19)$$

with the symplectic constraint

$$R_c^\top J R_c = J, \quad \mathbf{A} = R_c^\top J \mathbf{C}, \quad (20)$$

where R_c is also the 4-by-4 block, and \mathbf{C} is the crab dispersion generator.

The block diagonalized matrix $\bar{\mathcal{R}}_{\text{cav}}$ is

$$\bar{\mathcal{R}}_{\text{cav}} = \begin{bmatrix} \bar{R}_c & \mathbf{0}_{4 \times 1} & \mathbf{0}_{4 \times 1} \\ \mathbf{0}_{1 \times 4} & 1 & 0 \\ \mathbf{0}_{1 \times 4} & \bar{r}_{65} & 1 \end{bmatrix}, \quad (21)$$

with the symplectic constraint

$$\bar{R}_c^\top J \bar{R}_c = J. \quad (22)$$

Substituting Eqs. (7), (19), and (21) into Eq. (11), it follows that

$$\begin{aligned} \eta_2 &= R_c \eta_1 \\ \zeta_2 &= R_c \zeta_1 + \mathbf{C} - \frac{(r_{65} + \mathbf{A}^\top \zeta_1) \eta_2}{1 + (J\zeta_1)^\top \eta_1 + \mathbf{A}^\top \eta_1}. \end{aligned} \quad (23)$$

When $\boldsymbol{\eta}_1 = \mathbf{0}_{4 \times 1}$, the propagation turns into

$$\boldsymbol{\xi}_2 = R_c \boldsymbol{\xi}_1 + \mathbf{C}, \quad \boldsymbol{\eta}_2 = \mathbf{0}_{4 \times 1}. \quad (24)$$

Equations (13) and (19) include the most common accelerator components in a real machine. For a one-turn map in which both momentum dispersion generator \mathbf{D} and crab dispersion generator \mathbf{C} are present, the closed orbit condition is imposed on the two dispersion functions

$$\boldsymbol{\eta}_1 = \boldsymbol{\eta}_2, \quad \boldsymbol{\xi}_1 = \boldsymbol{\xi}_2. \quad (25)$$

This fixed point problem can be resolved with the help of Edwards-Teng approach [15,16].

To use the Edwards-Teng approach, the discussion is limited within the 4D phase space $\{x, p_x, z, \delta\}$. A general 4-by-4 transfer matrix in terms of 2-by-2 blocks is

$$R = \begin{bmatrix} R_{xx} & R_{xz} \\ R_{zx} & R_{zz} \end{bmatrix}. \quad (26)$$

Following [17], R is block diagonalized by

$$R = VUV^{-1} \quad (27)$$

with

$$V = \begin{bmatrix} g\mathbf{1}_{2 \times 2} & W \\ -W^+ & g\mathbf{1}_{2 \times 2} \end{bmatrix}, \quad U = \begin{bmatrix} U_{xx} & \mathbf{0}_{2 \times 2} \\ \mathbf{0}_{2 \times 2} & U_{zz} \end{bmatrix}, \quad (28)$$

where W, U_{xx}, U_{zz} are 2-by-2 blocks, W^+ is the symplectic conjugate of W , and g is given by

$$g^2 + (\det W) = 1, \quad (29)$$

where ‘‘det’’ means taking the determinant. This paper does not include the concrete formula of W , which the reader can find in [17].

With the closed orbit condition, Eq. (11) turns into

$$\mathcal{R} = \mathcal{M}\bar{\mathcal{R}}\mathcal{M}^{-1}. \quad (30)$$

Comparing it with Eq. (27), \mathcal{M} is related to V by a longitudinal scaling transformation, i.e.,

$$\mathcal{M} = \begin{bmatrix} g\mathbf{1}_{2 \times 2} & W \\ -W^+ & g\mathbf{1}_{2 \times 2} \end{bmatrix} \cdot \begin{bmatrix} P & \mathbf{0}_{2 \times 1} & \mathbf{0}_{2 \times 1} \\ \mathbf{0}_{1 \times 2} & 1/g & 0 \\ \mathbf{0}_{1 \times 2} & 0 & g \end{bmatrix}, \quad (31)$$

where P is a 2-by-2 matrix. From Eq. (31), the two kinds of closed orbit dispersion are

$$[\boldsymbol{\xi}, \boldsymbol{\eta}] = W \begin{bmatrix} 1/g & 0 \\ 0 & g \end{bmatrix} \quad (32)$$

and the matrix P follows

$$W^+P = \begin{bmatrix} g & 0 \\ 0 & 1/g \end{bmatrix} W^+. \quad (33)$$

The crab dispersion and the momentum dispersion at any point are related to the closed orbit form in Eq. (25) by the propagation formulas [Eqs. (17) and (23)]. Equation (7) presents a technique to decouple the transverse and the longitudinal phase space following acknowledgment of the two types of dispersion.

III. APPLICATIONS WITHOUT BEAM-BEAM

In this section, the subscript ‘‘b’’ denotes before IP, whereas the subscript ‘‘a’’ denotes after IP. Without loss of generality, our discussion focuses in the 4D phase space $\{x, p_x, z, \delta\}$. The propagation of the crab dispersion and the momentum dispersion does not involve the vertical plane. The lattice is assumed symmetrical around IP. The crab cavity before IP (CCB) and the crab cavity after IP (CCA) are placed at $\alpha_x = 0$, as shown in Fig. 2.

A. Nonzero momentum dispersion at crab cavities

When the crab cavities are turned off, the momentum dispersion vanishes at IP. Let the momentum dispersion at CCB be $(d, d')^T$. Then the transfer matrix from CCB to IP is

$$\mathcal{R}_b = \begin{bmatrix} 0 & \Lambda & 0 & -\Lambda d' \\ -1/\Lambda & 0 & 0 & d/\Lambda \\ d' & -d & 1 & r_{56} \\ 0 & 0 & 0 & 1 \end{bmatrix}, \quad (34)$$

where $\Lambda = \sqrt{\beta\beta^*}$, β , and β^* are the horizontal beta functions at crab cavities and IP. From the symmetry of the lattice, the

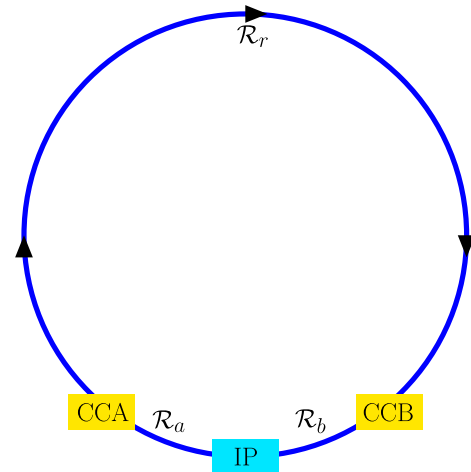


FIG. 2. The local crabbing scheme in a storage ring. ‘‘CCB’’ stands for the crab cavity before IP, and \mathcal{R}_b is the transfer matrix from CCB to IP. ‘‘CCA’’ stands for the crab cavity after IP, and \mathcal{R}_a is the transfer matrix from IP to CCA. \mathcal{R}_r is the transfer matrix from CCA to CCB.

momentum dispersion at CCA is $(d, -d')^T$, and the transfer matrix from IP to CCA is

$$\mathcal{R}_a = \begin{bmatrix} 0 & \Lambda & 0 & d \\ -1/\Lambda & 0 & 0 & -d' \\ -d/\Lambda & \Lambda d' & 1 & r_{56} \\ 0 & 0 & 0 & 1 \end{bmatrix}. \quad (35)$$

The periodic transfer matrix at IP should be

$$\begin{aligned} \mathcal{R}_{t1} &= \mathcal{R}_b \mathcal{R}_r \mathcal{R}_a \\ &= \begin{bmatrix} \cos \mu_x & \beta^* \sin \mu_x & 0 & 0 \\ -\frac{\sin \mu_x}{\beta^*} & \cos \mu_x & 0 & 0 \\ 0 & 0 & \cos \mu_z & \frac{\sigma_z \sin \mu_z}{\sigma_\delta} \\ 0 & 0 & -\frac{\sigma_\delta \sin \mu_z}{\sigma_z} & \cos \mu_z \end{bmatrix}, \end{aligned} \quad (36)$$

where \mathcal{R}_r is the transfer matrix from CCA to CCB, μ_x/μ_z is the periodic phase advance in horizontal/longitudinal plane, σ_z is the rms bunch length, and σ_δ is the rms momentum spread.

When the crab cavities are turned on, from Eq. (1), the linear transfer matrix of CCB and CCA are

$$\mathcal{C}_b = \begin{bmatrix} 1 & 0 & 0 & 0 \\ 0 & 1 & -\lambda_b & 0 \\ 0 & 0 & 1 & 0 \\ -\lambda_b & 0 & 0 & 1 \end{bmatrix}, \quad \mathcal{C}_a = \begin{bmatrix} 1 & 0 & 0 & 0 \\ 0 & 1 & -\lambda_a & 0 \\ 0 & 0 & 1 & 0 \\ -\lambda_a & 0 & 0 & 1 \end{bmatrix}, \quad (37)$$

where λ_b and λ_a are the strength of the crab cavity.

Starting with

$$\xi_0 = (0, 0)^T, \quad \eta_0 = (0, 0)^T \quad (38)$$

after transported to CCB by \mathcal{R}_b^{-1} , deflected by \mathcal{C}_b , and transported back to IP by \mathcal{R}_b , the crab dispersion and the momentum dispersion before collision read,

$$\begin{aligned} \xi_b &= \left(-\frac{\Lambda \lambda_b}{1 + \lambda_b d}, 0 \right)^T, \\ \eta_b &= (1 + \lambda_b d) \lambda_b d \left(\Lambda d', -\frac{d}{\Lambda} \right)^T + r_{56} (1 - \lambda_b d) (\Lambda \lambda_b, 0)^T \end{aligned} \quad (39)$$

Expanding Eq. (39) to the first order of λ_b ,

$$\begin{aligned} \xi_b &\approx (-\Lambda \lambda_b, 0)^T, \\ \eta_b &\approx \Lambda \lambda_b \left(dd' + r_{56}, -\frac{d^2}{\beta \beta^*} \right)^T. \end{aligned} \quad (40)$$

The Lorentz boost in Eq. (10) will cancel the crab dispersion when $\lambda_b = \theta_c/\Lambda$. However, the momentum dispersion does not vanish when $d \neq 0$ or $d' \neq 0$. Therefore, the horizontal coordinate x will depend on the momentum spread δ in the head-on frame, as shown in Fig. 3.

Due to the nonzero dispersion, the transverse coordinates relate to the momentum spread in the head-on frame by

$$\mathbf{X} = \bar{\mathbf{X}} + \eta_b \bar{\delta}, \quad \delta = \bar{\delta}. \quad (41)$$

The dispersion η_b can then be calculated from the second order moments as

$$\eta_{b,x} = \frac{\langle x, \delta \rangle}{\sigma_\delta^2}, \quad \eta_{b,p_x} = \frac{\langle p_x, \delta \rangle}{\sigma_\delta^2}, \quad (42)$$

where $\langle \cdot \rangle$ denotes taking the average over the particle distribution. Figure 4 compares the dispersion calculated from the analytic formula [Eq. (40)] and from the beam distribution [Eq. (42)].

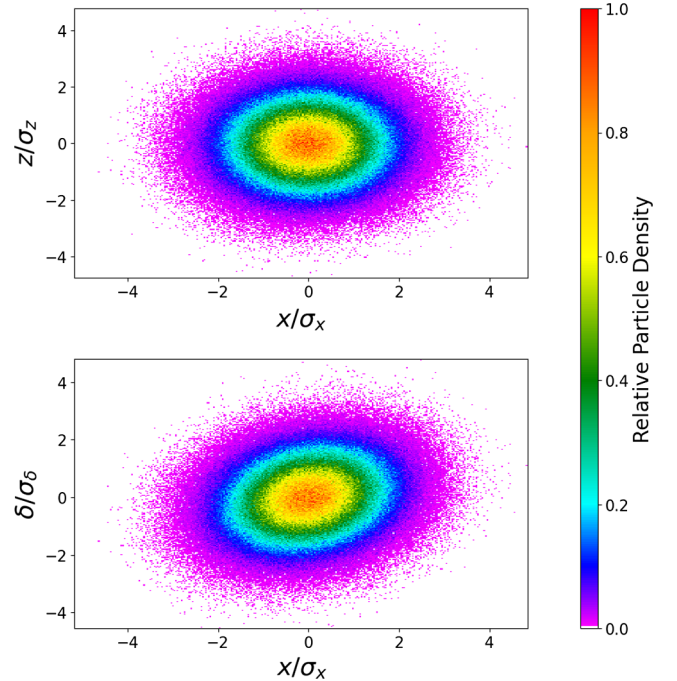


FIG. 3. Beam distribution before collision in x - z (top) and x - δ (bottom) plane. Both horizontal and vertical axes are normalized by rms beam size. The dispersion at the crab cavity is $d = 1$ m, $d' = 1$. The half crossing angle is $\theta_c = 12.5$ mrad. The r_{56} element from CCB to IP is chosen as $r_{56} = 2$ m. The crab cavity strength is determined by $\lambda_b = \theta_c/\Lambda$. The horizontal beta functions at IP and the crab cavity are $\beta^* = 0.5$ m, $\beta = 200$ m.

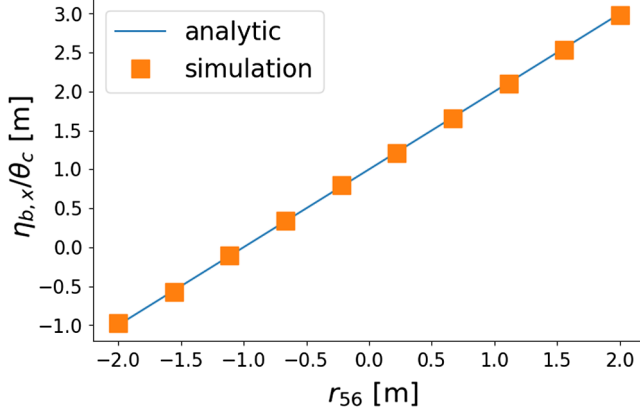


FIG. 4. The horizontal momentum dispersion in the head-on frame versus the r_{56} element from CCB to IP. The analytic line (blue) is obtained from Eq. (40), and the simulation data (yellow) are obtained from the statistics of the beam distribution. Other parameters are same as in Fig. 3.

Projecting the crab dispersion and the momentum dispersion at the other side back to IP, it follows

$$\begin{aligned}\xi_a &= \left(\frac{\Lambda \lambda_a}{1 + \lambda_a d}, 0 \right)^T, \\ \eta_a &= (1 + \lambda_a d) \lambda_a d \left(\Lambda d', \frac{d}{\Lambda} \right)^T + r_{56} (1 - \lambda_a d) (\Lambda \lambda_a, 0)^T.\end{aligned}\quad (43)$$

Expanding Eq. (43) to the first order of λ_a ,

$$\begin{aligned}\xi_a &\approx (\Lambda \lambda_a, 0)^T, \\ \eta_a &\approx \Lambda \lambda_a \left(dd' + r_{56}, \frac{d^2}{\beta \beta^*} \right)^T.\end{aligned}\quad (44)$$

Taking both sides into consideration, the crab dispersion can be closed when

$$\lambda_b = \lambda_a \approx \theta_c / \Lambda. \quad (45)$$

Then the residual momentum dispersion is

$$\eta_a + \eta_b \approx 2\theta_c (dd' + r_{56}, 0)^T. \quad (46)$$

The leakage of the momentum dispersion will lead to the coupling between the horizontal and longitudinal plane, and it is necessary to consider the closed orbit form of the two types of distribution.

Define

$$k_\eta \equiv 2\theta_c (dd' + r_{56}). \quad (47)$$

With both crab cavities on, the periodic transfer matrix at IP is

$$\begin{aligned}\mathcal{R}_{12} &= (\mathcal{R}_b \mathcal{R}_r \mathcal{R}_a) (\mathcal{R}_a^{-1} \mathcal{C}_a \mathcal{R}_a) (\mathcal{R}_b \mathcal{C}_b \mathcal{R}_b^{-1}) \\ &\approx \mathcal{R}_{t1} \begin{bmatrix} 1 & 0 & 0 & k_\eta \\ 0 & 1 & 0 & 0 \\ 0 & k_\eta & 1 & 0 \\ 0 & 0 & 0 & 1 \end{bmatrix} \\ &= \begin{bmatrix} \cos \mu_x & \beta^* \sin \mu_x & 0 & k_\eta \cos \mu_x \\ -\frac{\sin \mu_x}{\beta^*} & \cos \mu_x & 0 & -\frac{k_\eta \sin \mu_x}{\beta^*} \\ 0 & k_\eta \cos \mu_z & \cos \mu_z & \frac{\sigma_z \sin \mu_z}{\sigma_\delta} \\ 0 & -\frac{k_\eta \sigma_\delta \sin \mu_z}{\sigma_z} & -\frac{\sigma_\delta \sin \mu_z}{\sigma_z} & \cos \mu_z \end{bmatrix}.\end{aligned}\quad (48)$$

Following the procedure in [17], we define

$$\begin{aligned}H &= \begin{bmatrix} -\frac{k_\eta \sigma_\delta \sin \mu_z}{\sigma_z} & k_\eta (\cos \mu_x - \cos \mu_z) \\ 0 & -\frac{k_\eta \sin \mu_x}{\beta^*} \end{bmatrix}, \\ g &= \sqrt{\frac{1}{2} + \frac{1}{2} \sqrt{\frac{(\cos \mu_x - \cos \mu_z)^2}{(\cos \mu_x - \cos \mu_z)^2 + \det H}}},\end{aligned}\quad (49)$$

and then

$$W = \frac{H}{2g \sqrt{(\cos \mu_x - \cos \mu_z)^2 + \det H}}. \quad (50)$$

The stability criterion is

$$(\cos \mu_x - \cos \mu_z)^2 + \frac{k_\eta^2 \sin \mu_x \sin \mu_z}{\beta^* \sigma_z / \sigma_\delta} > 0. \quad (51)$$

Similar to the betatron resonance, the sum resonance $\mu_x + \mu_z = 0$ is dangerous, while the motion on difference resonance $\mu_x - \mu_z = 0$ is stable. However, the longitudinal average action is usually much larger than the horizontal rms emittance, the coupling has to be weak enough to prevent the luminosity loss,

$$g \approx 1, \quad W \approx \frac{H}{2|\cos \mu_x - \cos \mu_z|}. \quad (52)$$

From Eq. (32), the two kinds of closed orbit dispersion are

$$\begin{aligned}\zeta_{\text{co},x} &= -\frac{k_\eta \sin \mu_z}{2|\cos \mu_x - \cos \mu_z| \sigma_z / \sigma_\delta} \\ \eta_{\text{co},x} &= \frac{1}{2} k_\eta \text{sgn}(\cos \mu_x - \cos \mu_z),\end{aligned}\quad (53)$$

where

$$\text{sgn}(x) = \begin{cases} -1, & \text{for } x \leq 0 \\ +1, & \text{for } x > 0 \end{cases}. \quad (54)$$

To prevent the horizontal beam size blows up,

$$|\zeta_{\text{co},x}| \ll \frac{\sigma_x}{\sigma_z}, \quad |\eta_{\text{co},x}| \ll \frac{\sigma_x}{\sigma_\delta}, \quad (55)$$

so that the constraints are given by

$$\left| \frac{k_\eta}{2} \right| \ll \frac{\sigma_x |\cos \mu_x - \cos \mu_z|}{\sigma_\delta \sin \mu_z} \quad (56)$$

and

$$\left| \frac{k_\eta}{2} \right| \ll \frac{\sigma_x}{\sigma_\delta}. \quad (57)$$

From Eq. (47), k_η and θ_c are within the same order of magnitude. As a result, the constraint of Eq. (57) is generally satisfied. However, when μ_x is close to μ_z , even if the stability criterion Eq. (51) holds, the constraint of Eq. (56) may be broken. In other words, the leakage of momentum dispersion will result in a significant closed orbit crab dispersion, and the luminosity will be reduced hereafter.

The theory is verified by tracking. The macroparticles are randomly generated at IP from the Gaussian distribution,

$$\rho(x, p_x, z, \delta) = \frac{1}{(2\pi)^2 \sigma_x \sigma_{p_x} \sigma_z \sigma_\delta} \times \exp\left(-\frac{x^2}{2\sigma_x^2} - \frac{p_x^2}{\sigma_{p_x}^2} - \frac{z^2}{2\sigma_z^2} - \frac{\delta^2}{2\sigma_\delta^2}\right). \quad (58)$$

The parameters are listed in Table I. The working point is chosen close to the difference resonance. The sinusoidal kick Eq. (1) from the crab cavities is used during tracking. Figure 5 presents the beam size evolution caused by the momentum distribution leakage. In our model, all elements are linear except for the crab cavities. As a result, the beam envelope oscillates. The oscillation amplitude is determined

TABLE I. Initial beam size and crab cavity parameters in the tracking of dispersion leakage.

Parameter	Unit	Value
Horizontal size σ_x	μm	95
Horizontal divergence σ_{p_x}	μrad	211
Longitudinal size σ_z	cm	2
Momentum spread σ_δ	10^{-4}	5.5
Horizontal β at IP	m	0.45
Horizontal β at crab cavity	m	222
Crab cavity frequency	MHz	200
Crab cavity phase	rad	0
Half crossing angle θ_c	mrاد	12.5

by k_η in Eq. (47) or $dd' + r_{56}$ to the first order, which leads to the yellow, green, and red curves overlap with each other. When the horizontal tune ν_x is close to the longitudinal tune ν_z , the motion is still stable, but the envelope oscillation amplitude becomes much larger. If the coupling is weak enough, the oscillation frequency is determined by $|\nu_x - \nu_z|$ [13]. The envelope oscillation will lead to the horizontal beam size blowup when the nonlinearity is present, such as the beam-beam interaction, the chromaticity, or high-order magnetic fields.

From Fig. 5, the horizontal size reaches maximum at about 500th turn. Figure 6 shows the beam distribution in x - z and x - δ plane at that moment. It demonstrates that the horizontal coordinate is substantially associated with the longitudinal coordinate z , but weakly depending on the momentum spread δ . It proves that the closed orbit crab dispersion is significantly bigger than the momentum dispersion when the horizontal tune is close to the longitudinal tune.

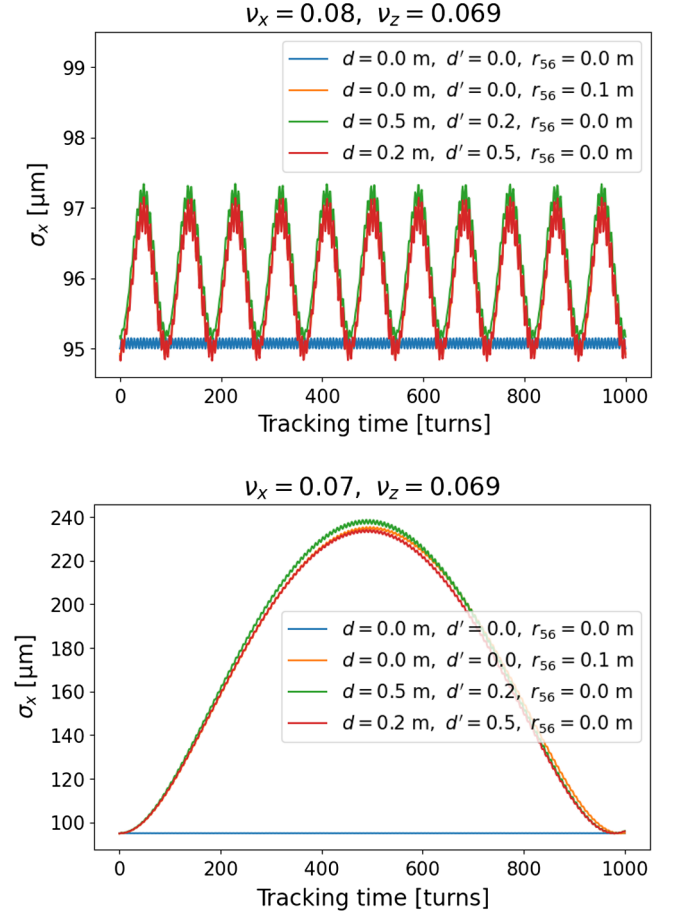


FIG. 5. The horizontal beam size evolution due to the momentum distribution leakage. ν_x is the horizontal tune, ν_z the longitudinal tune, and (d, d') the horizontal momentum dispersion at the crab cavities when the crab cavities are turned off. r_{56} is the matrix element from CCB to IP, or from IP to CCA.

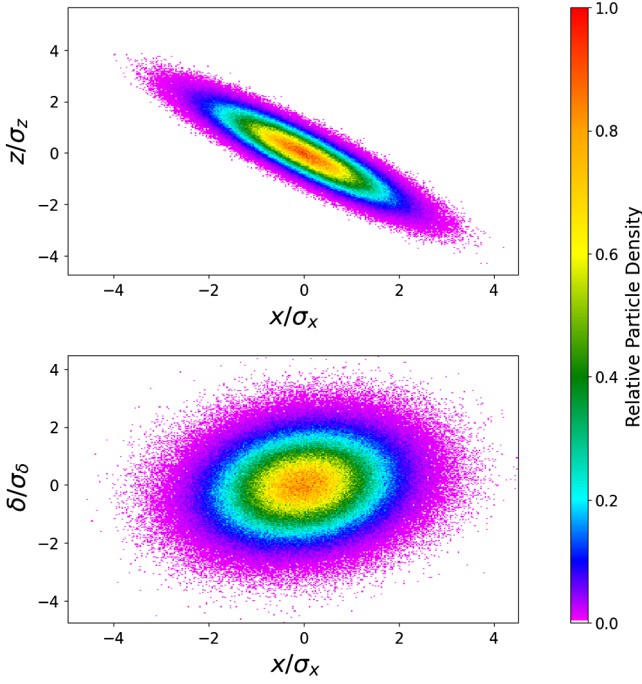


FIG. 6. Beam distribution in x - z (top) and x - δ (bottom) plane at 500th turn for the green curve in the bottom of Fig. 5. Both horizontal and vertical axes are normalized by rms beam size.

B. Nonideal phase from crab cavities to IP

The crab dispersion from the crab cavities at both sides will cancel with each other when the horizontal phase advance from the crab cavity to IP is exactly $\pi/2$. However, this is not always true in IR design. As a result, the crab dispersion will leak out of IR.

Let Ψ_b be the horizontal phase from CCB to IP, and Ψ_a is the horizontal phase from IP to CCA. The β functions at both crab cavities are still assumed identical. We also omit the momentum dispersion in this section to simplify our discussion. The transfer matrices between the crab cavities and IP are given by

$$\mathcal{R}_b = \begin{bmatrix} \frac{\beta^*}{\Lambda} \cos \Psi_b & \Lambda \sin \Psi_b & 0 & 0 \\ -\frac{\sin \Psi_b}{\Lambda} & \frac{\Lambda}{\beta^*} \cos \Psi_b & 0 & 0 \\ 0 & 0 & 1 & 0 \\ 0 & 0 & 0 & 1 \end{bmatrix},$$

$$\mathcal{R}_a = \begin{bmatrix} \frac{\Lambda}{\beta^*} \cos \Psi_a & \Lambda \sin \Psi_a & 0 & 0 \\ -\frac{\sin \Psi_a}{\Lambda} & \frac{\beta^*}{\Lambda} \cos \Psi_a & 0 & 0 \\ 0 & 0 & 1 & 0 \\ 0 & 0 & 0 & 1 \end{bmatrix}. \quad (59)$$

Following the same procedure in Sec. III A, the crab dispersion before collision is

$$\xi_b = -\Lambda \lambda_b \left(\sin \Psi_b, \frac{\cos \Psi_b}{\beta^*} \right)^T \quad (60)$$

when $\Psi_b \neq \pi/2$, the second term in ξ_b will not be equal to 0. It will introduce additional synchro-betatron resonance and will degrade the beam-beam performance.

Projecting the crab dispersion from CCA back to IP,

$$\xi_a = -\Lambda \lambda_a \left(-\sin \Psi_a, \frac{\cos \Psi_a}{\beta^*} \right)^T. \quad (61)$$

It is easy to show that the residual crab dispersion vanishes when

$$\Psi_b + \Psi_a = \pi, \quad \lambda_a = \lambda_b = \frac{\theta_c}{\Lambda \sin \Psi_b}. \quad (62)$$

There will be a leakage of crab dispersion when the total phase $\Psi_b + \Psi_a$ deviates from π .

Let

$$\lambda_b = \frac{\theta_c}{\Lambda \sin \Psi_b}, \quad \lambda_a = \frac{\theta_c}{\Lambda \sin \Psi_a}. \quad (63)$$

Then the leakage of the crab dispersion will be

$$\xi_a + \xi_b = \theta_c \left(0, -\frac{\cot \Psi_a + \cot \Psi_b}{\beta^*} \right)^T. \quad (64)$$

Define

$$k_\zeta \equiv -\theta_c \left(\frac{\cot \Psi_a + \cot \Psi_b}{\beta^*} \right). \quad (65)$$

With the crab dispersion leakage, the periodic transfer matrix at IP is

$$\begin{aligned} \mathcal{R}_{I3} &= (\mathcal{R}_b \mathcal{R}_r \mathcal{R}_a) (\mathcal{R}_a^{-1} \mathcal{C}_a \mathcal{R}_a) (\mathcal{R}_b \mathcal{C}_b \mathcal{R}_b^{-1}) \\ &= \mathcal{R}_{I1} \begin{bmatrix} 1 & 0 & 0 & 0 \\ 0 & 1 & k_\zeta & 0 \\ 0 & 0 & 1 & 0 \\ k_\zeta & 0 & 0 & 1 \end{bmatrix} \\ &= \begin{bmatrix} \cos \mu_x & \beta^* \sin \mu_x & \beta^* k_\zeta \sin \mu_x & 0 \\ -\frac{\sin \mu_x}{\beta^*} & \cos \mu_x & k_\zeta \cos \mu_x & 0 \\ \frac{k_\zeta \sigma_z \sin \mu_z}{\sigma_\delta} & 0 & \cos \mu_z & \frac{\sigma_z \sin \mu_z}{\sigma_\delta} \\ k_\zeta \cos \mu_z & 0 & -\frac{\sigma_\delta \sin \mu_z}{\sigma_z} & \cos \mu_z \end{bmatrix}. \end{aligned} \quad (66)$$

The stability criterion becomes

$$(\cos \mu_x - \cos \mu_z)^2 + k_\zeta^2 \sin \mu_x \sin \mu_z \beta^* (\sigma_z / \sigma_\delta) > 0. \quad (67)$$

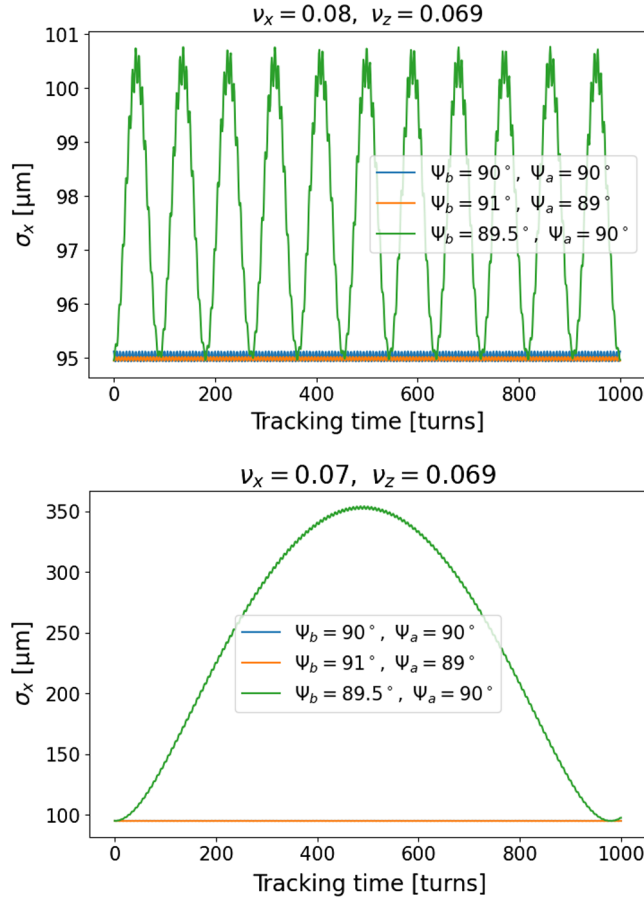


FIG. 7. The horizontal beam size evolution due to the crab distribution leakage. ν_x is the horizontal tune and ν_z is the longitudinal tune. Ψ_b is the horizontal phase advance from CCB to IP and Ψ_a is the horizontal phase advance from IP to CCA.

Assuming the longitudinal-horizontal coupling is weak enough, the two kinds of closed orbit dispersion are

$$\zeta_{\text{co},x} = \frac{\beta^* k_\zeta \sin \mu_x}{2 |\cos \mu_x - \cos \mu_z|}, \quad \eta_{\text{co},x} = 0. \quad (68)$$

Then a constraint is given by

$$\left| \frac{k_\zeta}{2} \right| \ll \frac{\sigma_x |\cos \mu_x - \cos \mu_z|}{\beta^* \sigma_z \sin \mu_x}. \quad (69)$$

The bunch length σ_z is usually much larger than the transverse size σ_x . Accordingly, Eq. (69) places a strict constraint on k_ζ .

Figure 7 presents the beam size evolution caused by the crab distribution leakage. The simulation parameters are listed in Table I. We can see that even 0.5° deviation from π driving a notable envelope oscillation for the tunes $\nu_x = 0.07$ and $\nu_z = 0.069$. Figure 8 shows the distribution in $x-z$ and $x-\delta$ plane when the horizontal envelope reaches maximum. It turns out that it is the closed orbit crab

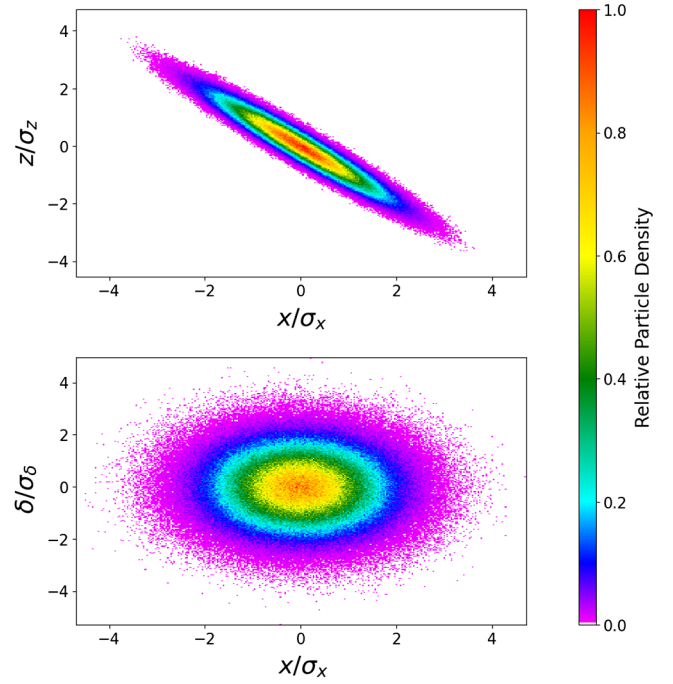


FIG. 8. Beam distribution in $x-z$ (top) and $x-\delta$ (bottom) plane at 500th turn for the green curve in the bottom of Fig. 7. Both horizontal and vertical axes are normalized by rms beam size.

dispersion dominated the envelope oscillation, as predicted by Eq. (68).

IV. APPLICATIONS WITH BEAM-BEAM

The leakage of the crab dispersion and momentum dispersion will impose additional constraints on the lattice design. Weak-strong simulation is a widely used approach in beam-beam study [18,19]. In this part, we will investigate the influence of dispersion leakage on beam-beam performance using a self-written weak-strong code.

Table II presents the beam parameters used in the simulation to demonstrate the combined effects of crab dispersion and momentum dispersion. In the simulation, the ion beam is rigid with the horizontal centroid as [11]

$$x_i = -\theta_c \left[\frac{4 \sin(k_{c,i}z)}{3 k_{c,i}} - \frac{1 \sin(2k_{c,i}z)}{3 2k_{c,i}} - z \right], \quad (70)$$

where $k_{c,i}$ is the wave number of the crab cavities in the ion ring. A second order harmonic crab cavity is used to flatten the ion bunch in the head-on frame. The ion bunch is cut into multiple slices. Each slice is represented by a 2D Gaussian distribution in $x-y$ plane.

The weak electron beam is simulated by a number of macroparticles. As in Secs. III A and III B, both the one-turn map and the betatron map from the crab cavities to IP are described by the linear transfer matrix. The crab cavity kick follows Eq. (1). The beam-beam kick from a Gaussian distribution is calculated with the Bassetti and Erskine

TABLE II. Beam parameters in weak-strong simulation. The parameters come from EIC Conceptual Design Report [5].

Parameter	Proton	Electron
Circumference [m]	3833.8	
Energy [GeV]	275	10
Particles per bunch [10^{11}]	0.6881	1.7203
Crossing angle [mrad]	25	
Crab cavity frequency [MHz]	200	400
β_x^*/β_y^* [cm]	80/7.20	55/5.6
RMS emittance (H/V)[nm]	11.3/1	20/1.30
RMS bunch size (H/V)[μm]	95/8.50	105/8.50
RMS bunch length [cm]	6	2
RMS energy spread [10^{-4}]	6.6	5.5
Transverse fractional tune (H/V)	0.228/0.210	0.08/0.06
Synchrotron tune	0.010	0.069
Transverse damping time [turns]	∞	4000
Longitudinal damping time [turns]	∞	2000
Beam-beam parameter (H/V)	0.009/0.009	0.09/0.10

formula [20]. The effects of radiation damping and quantum excitation are represented by a lumped element [21].

Figure 9 shows the beam size evolution without any dispersion leakage. Compared with the nominal working point, $\nu_x = 0.08$, $\nu_y = 0.06$, in the EIC Conceptual Design

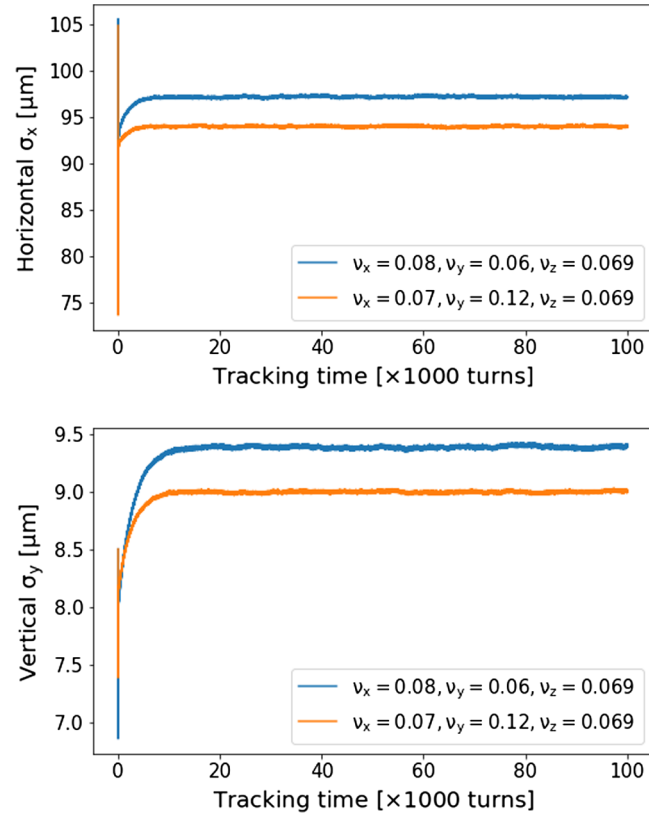


FIG. 9. Weak-strong simulation results for the case without any dispersion leakage. The ν_x , ν_y , ν_z are horizontal, vertical and longitudinal tunes, respectively.

Report, the new working point, $\nu_x = 0.07$, $\nu_y = 0.12$, predicts smaller horizontal and vertical beam sizes after equilibrium. The horizontal size benefits from the smaller horizontal tune which reduces the dynamical β_x under beam-beam interaction [22]. The vertical size benefits from a larger difference $|\nu_x - \nu_y|$ so that the new working point moves away from the main diagonal line in the tune space. From the viewpoint of beam-beam, the new working point, $\nu_x = 0.07$, $\nu_y = 0.12$, is a better choice.

A. Nonzero momentum dispersion at crab cavities

Figure 10 presents the final beam sizes after equilibrium with different momentum dispersion d and d' at both crab cavities. The r_{56} term from CCB (IP) to IP (CCA) is set to 0 in all simulations. Compared with the simulations without beam-beam interaction in Sec. III A, Figure 10 shows a quite different pattern. The vertical size after equilibrium is also affected due to the nonlinearity from the beam-beam interaction. The horizontal blowup is less severe even for the new working point where the horizontal tune $\nu_x = 0.07$ is quite close to the longitudinal tune $\nu_z = 0.069$. The equilibrium size is mainly determined by d' instead of $dd' + r_{56}$.

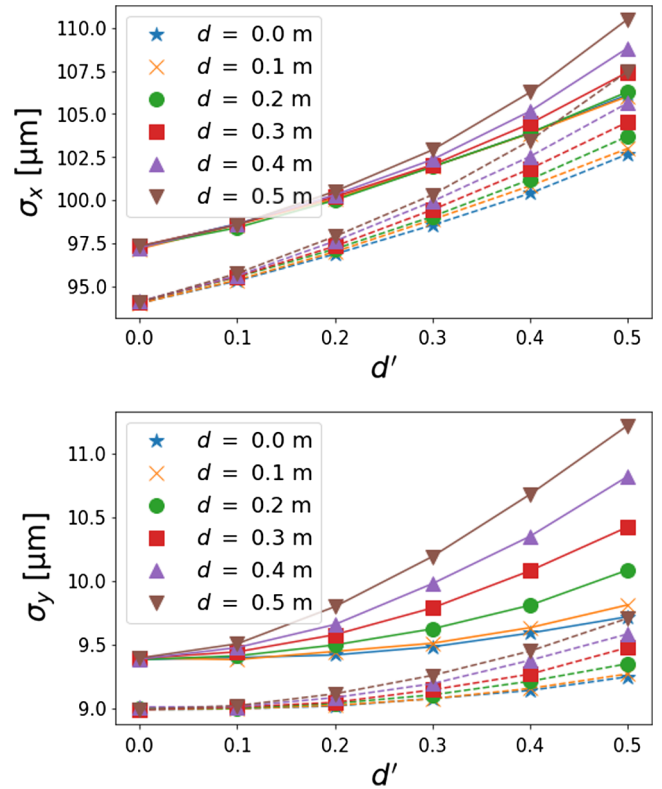


FIG. 10. Weak-strong simulation results for different d and d' . (d , d') is the horizontal momentum dispersion at CCB when the crab cavities are turned off. The solid curves are for the working point (0.08,0.06,0.069), whereas the dashed curves are for (0.07,0.12,0.069). The horizontal size σ_x and the vertical size σ_y are averaged from the last 1000 turns.

The reason is that the horizontal tune and β function are modified by the beam-beam interaction. With the near axis approximation, the beam-beam kick can be represented by a linear quadrupole in the head-on frame,

$$\mathcal{B} = \begin{bmatrix} 1 & 0 & 0 & 0 \\ -1/f_x & 1 & 0 & 0 \\ 0 & 0 & 1 & 0 \\ 0 & 0 & 0 & 1 \end{bmatrix}, \quad (71)$$

where f_x is the horizontal focal length and can be expressed with the beam-beam parameter ξ_x by

$$\frac{1}{f_x} = \frac{4\pi\xi_x}{\beta^*}. \quad (72)$$

For simplicity, the vertical dynamics is not included here. Back into the Frenet-Serret frame, the linear beam-beam transformation is given by

$$\mathcal{L}^{-1}\mathcal{B}\mathcal{L} = \begin{bmatrix} 1 & 0 & 0 & 0 \\ -1/f_x & 1 & -\theta_c/f_x & 0 \\ 0 & 0 & 1 & 0 \\ -\theta_c/f_x & 0 & -\theta_c^2/f_x & 1 \end{bmatrix}, \quad (73)$$

where \mathcal{L} is the linear Lorentz boost, as shown in Eq. (9).

Turning the crab cavities on, the total transfer matrix including the crab system and the beam-beam interaction follows:

$$\begin{aligned} \mathcal{R}_{\text{bb}} &= (\mathcal{R}_a^{-1}\mathcal{C}_a\mathcal{R}_a)(\mathcal{L}^{-1}\mathcal{B}\mathcal{L})(\mathcal{R}_b\mathcal{C}_b\mathcal{R}_b^{-1}) \\ &\approx \begin{bmatrix} 1 - a_x & a_x^2 f_x & 0 & k_\eta \\ -\frac{1}{f_x} & 1 + a_x & 0 & -\frac{k_\eta}{2f_x} \\ -\frac{k_\eta}{2f_x}(1 + a_x) & k_\eta(1 + a_x + \frac{a_x^2}{2}) & 1 & 0 \\ 0 & 0 & 0 & 1 \end{bmatrix}, \end{aligned} \quad (74)$$

where

$$a_x = \frac{2\Lambda\theta_c d'}{f_x}. \quad (75)$$

Then the periodic transfer matrix is

$$\mathcal{R}_{t2,\text{bb}} = \mathcal{R}_{t1}\mathcal{R}_{\text{bb}}. \quad (76)$$

Due to $k_\eta \propto \theta_c$, the longitudinal-horizontal coupling is still weak. The horizontal dynamic tune and β are then given by

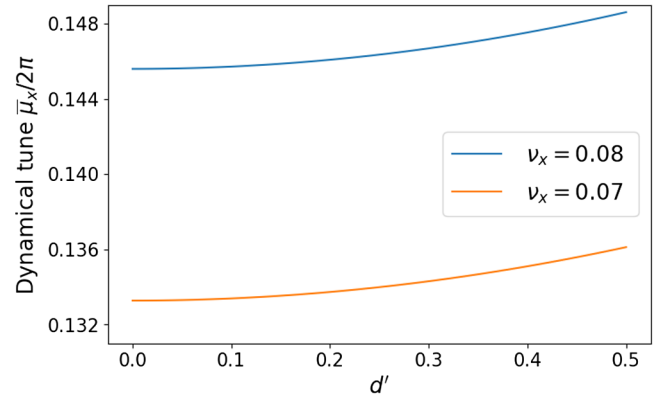


FIG. 11. Dynamical tune in the presence of beam-beam interaction. (d, d') is the horizontal momentum dispersion at CCB when the crab cavities are turned off.

$$\begin{aligned} \cos \bar{\mu}_x &= \cos \mu_x - \frac{1}{2} \left(\frac{\beta^*}{f_x} + \frac{a_x^2 f_x}{\beta^*} \right) \sin \mu_x \\ \bar{\beta}^* \sin \bar{\mu}_x &= a_x^2 f_x \cos \mu_x + \beta^* (1 + a_x) \sin \mu_x. \end{aligned} \quad (77)$$

Figure 11 shows the dynamical tune as a function of d' . For both working points, the horizontal tune with the beam-beam interaction is larger than 0.13, which is far enough away from the longitudinal tune 0.069. Therefore, the closed orbit of the momentum dispersion and crab dispersion is negligible. Figure 12 shows the dynamical beta as a function of d' . The dynamical beta increases as d' gets larger, which explains why the horizontal size depends mainly on d' instead of $dd' + r_{56}$.

It is worthwhile to mention that the dynamical beta is not the only source of beam size growth. The nonzero momentum dispersion d or d' at crab cavities will excite higher-order synchro-betatron resonances through the nonlinear beam-beam interaction.

In summary, from the weak-strong simulation, when the dispersion satisfies the constraints,

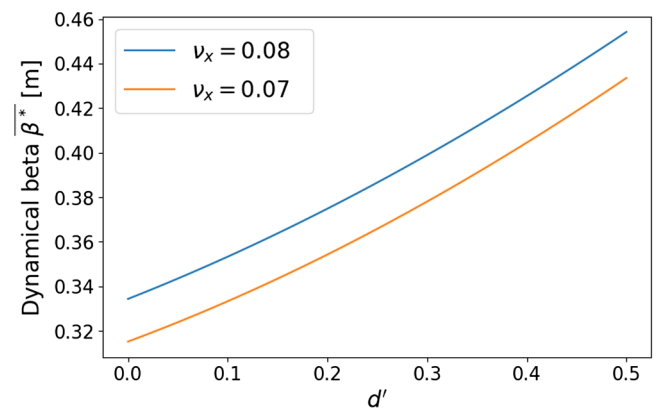


FIG. 12. Dynamical beta function in the presence of beam-beam interaction. (d, d') is the horizontal momentum dispersion at CCB when the crab cavities are turned off.

$$|d| < 0.5 \text{ m}, \quad d' \sim 0, \quad (78)$$

the beam size growth caused by the momentum dispersion is small. The closed orbit crab dispersion or momentum dispersion without beam-beam interaction is also negligible.

B. Nonideal phase from crab cavities to IP

For symplecticity, we still omit the momentum dispersion here. Substituting Eq. (73) into Eq. (23), the crab dispersion deflected by the beam-beam kick is

$$\begin{bmatrix} 1 & 0 \\ -1/f_x & 1 \end{bmatrix} \xi_b + \begin{bmatrix} 0 \\ -\theta_c/f_x \end{bmatrix} = \xi_b, \quad (79)$$

where ξ_b takes the form of Eq. (60), and the crab cavity strength is determined by Eq. (63). Because the beam-beam kick has no effect on crab dispersion, the criteria Eq. (69) still holds true, with the exception that the horizontal phase must be replaced by the dynamical phase

$$\left| \frac{k_z}{2} \right| \ll \frac{\sigma_x |\cos \bar{\mu}_x - \cos \mu_z|}{\beta^* \sigma_z \sin \mu_x} \quad (80)$$

or specifically,

$$|\cot \Psi_a + \cot \Psi_b| \leq \frac{\sigma_x |\cos \bar{\mu}_x - \cos \mu_z|}{5\sigma_z \theta_c \sin \mu_x}, \quad (81)$$

where the dynamical phase $\bar{\mu}_x$ is determined by Eq. (77), and the upper boundary is set as 1/10 in Eq. (80).

Let $\Psi_b = \Psi_a = \pi/2 - \Delta\Psi$. Then the criterion becomes numerically,

$$\begin{aligned} |\Delta\Psi| &\leq 0.80^\circ \quad \text{when } \nu_x = 0.08 \\ |\Delta\Psi| &\leq 0.58^\circ \quad \text{when } \nu_x = 0.07. \end{aligned} \quad (82)$$

Figures 13 and 14 show the weak-strong simulation results for different $\Delta\Psi$ at both working points. Both figures demonstrate that the constraint Eq. (82) has to be satisfied. Otherwise, the horizontal beam size will increase dramatically.

However, the constraint of Eq. (82) may be too strict to meet in reality because of the compact layout of the IR. A possible alternative is to move the crab cavities in one ring to the phase of $3\pi/2$ or further.

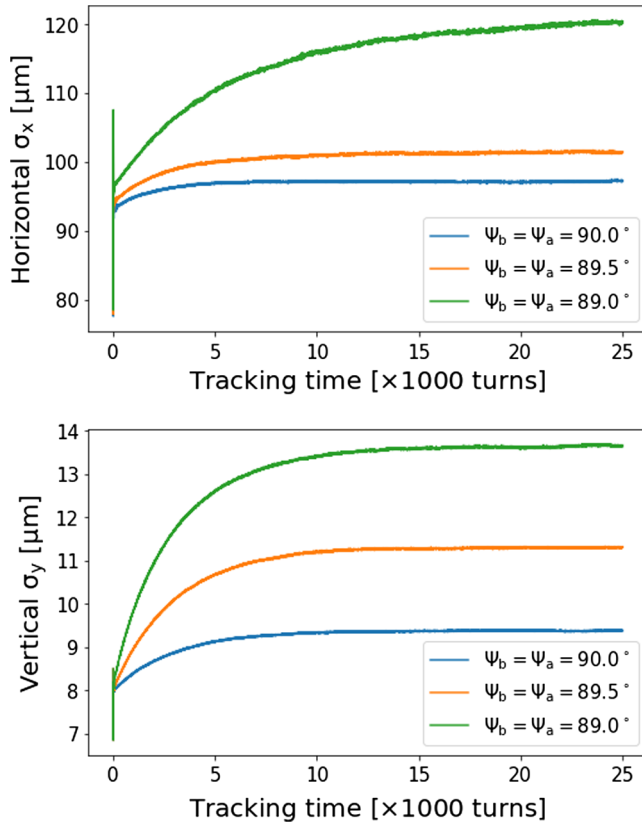


FIG. 13. Weak-strong simulation results with nonideal phase at the working point of (0.08,0.06,0.069). Ψ_b is the horizontal phase advance from CCB to IP and Ψ_a is the horizontal phase advance from IP to CCA.

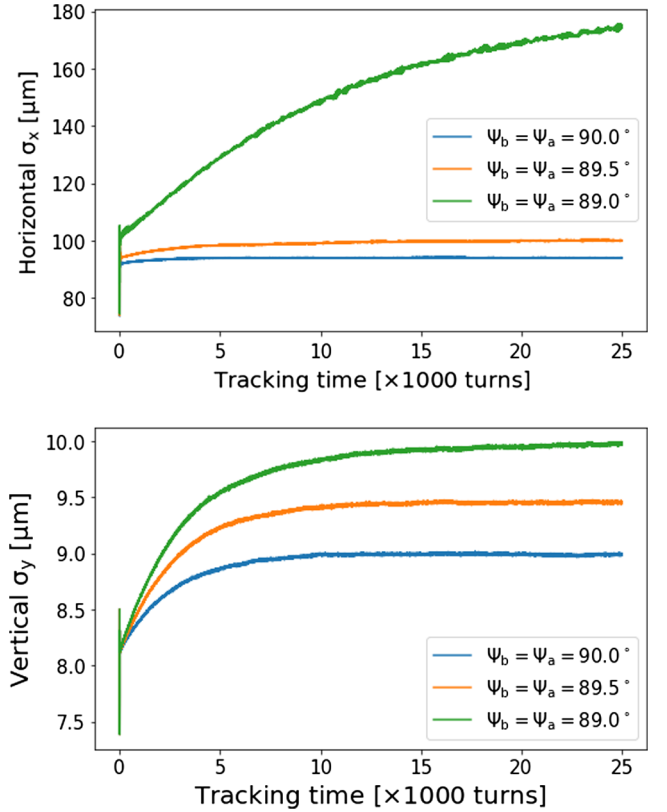


FIG. 14. Weak-strong simulation results with nonideal phase at the working point of (0.07,0.12,0.069). Ψ_b is the horizontal phase advance from CCB to IP and Ψ_a is the horizontal phase advance from IP to CCA.

V. CONCLUSION

In this study, we extended the concept of crab dispersion and momentum dispersion in the presence of synchrotron motion. We derived the propagation law of the two types of dispersion traveling via common accelerator elements. Edward-Teng's block diagonalization technique was also used to find the closed orbit form of dispersions. It enabled us to deduce the leakage of crab dispersion and momentum dispersion in the local crabbing scheme.

This paper then investigated the momentum dispersion at the crab cavities and the nonideal phase from the crab cavities to IP. The stability criterion was derived. A lattice requirement criterion was calculated using the weak horizontal-longitudinal coupling assumption. It turned out that the beam size at IP became sensitive to the leakage of dispersions when the horizontal tune was close to the longitudinal tune. The Monte Carlo simulations were carried out to demonstrate the theoretical analysis.

The beam-beam interaction was taken into consideration in the weak-strong simulations. It showed that the momentum dispersion at crab cavities had less impact on the beam size at IP because of the beam-beam tune shift. However, the phase advance from crab cavities to IP cannot stay too far from $\pi/2$. The numerical criteria of the electron ring lattice were given for the EIC beam parameters. The simulation results agreed with the criteria.

ACKNOWLEDGMENTS

This work was supported by Department of Energy under Contract No. DE-AC02-98CH10886.

-
- [1] R. Palmer, Energy scaling, crab crossing and the pair problem, Stanford Linear Accelerator Center, Technical Report No. SLAC-PUB-4707, 1988.
 - [2] K. Oide and K. Yokoya, Beam-beam collision scheme for storage-ring colliders, *Phys. Rev. A* **40**, 315 (1989).
 - [3] T. Abe, K. Akai, M. Akemoto, A. Akiyama, M. Arinaga, K. Ebihara, K. Egawa, A. Enomoto, J. Flanagan, S. Fukuda *et al.*, Compensation of the crossing angle with crab cavities at KEKB, in *Proceedings of the 2007 IEEE Particle Accelerator Conference, IPAC-2007, Albuquerque, NM* (IEEE, Piscataway, NJ, 2007), pp. 27–31.
 - [4] R. Calaga, A. Alekou, F. Antoniou, R. Appleby, L. Arnaudon, K. Artoos, G. Arduini, V. Baglin, S. Barriere, H. Bartosik *et al.*, First demonstration of the use of crab cavities on hadron beams, *Phys. Rev. Accel. Beams* **24**, 062001 (2021).
 - [5] J. Beebe-Wang *et al.*, Electron ion collider conceptual design report, Brookhaven National Laboratory, Technical Report No. BNL-221006-2021-FORE, 2021, [10.2172/1765663](https://arxiv.org/abs/10.2172/1765663).
 - [6] Y.-P. Sun, R. Assmann, R. Tomás, and F. Zimmermann, Crab dispersion and its impact on the CERN large hadron collider collimation, *Phys. Rev. ST Accel. Beams* **13**, 031001 (2010).
 - [7] X. Huang, Coupled beam motion in a storage ring with crab cavities, *Phys. Rev. Accel. Beams* **19**, 024001 (2016).
 - [8] G. H. Hoffstaetter and A. W. Chao, Synchrotron stop bands due to a single crab cavity, *Phys. Rev. ST Accel. Beams* **7**, 071002 (2004).
 - [9] Y.-P. Sun, R. Assmann, J. Barranco, R. Tomás, T. Weiler, F. Zimmermann, R. Calaga, and A. Morita, Beam dynamics aspects of crab cavities in the CERN large hadron collider, *Phys. Rev. ST Accel. Beams* **12**, 101002 (2009).
 - [10] Y. Funakoshi, Operational experience with crab cavities at KEKB, [arXiv:1410.4036](https://arxiv.org/abs/1410.4036).
 - [11] D. Xu, Y. Hao, Y. Luo, and J. Qiang, Synchrotron resonance of crab crossing scheme with large crossing angle and finite bunch length, *Phys. Rev. Accel. Beams* **24**, 041002 (2021).
 - [12] Y. H. Chin, Effects of non-zero dispersion at crab cavities on the beam dynamics (1990), <https://www.osti.gov/servlets/purl/6442988>.
 - [13] A. W. Chao, Lecture notes on topics in accelerator physics, Stanford Linear Accelerator Center, Menlo Park, CA, Technical Report No. SLAC-PUB-9574, 2002.
 - [14] K. Hirata, Analysis of Beam-Beam Interactions with a Large Crossing Angle, *Phys. Rev. Lett.* **74**, 2228 (1995).
 - [15] D. Edwards and L. Teng, Parameterization of linear coupled motion in periodic structures, *IEEE Trans. Nucl. Sci.* **20**, 885 (1973).
 - [16] K. Ohmi, K. Hirata, and K. Oide, From the beam-envelope matrix to synchrotron-radiation integrals, *Phys. Rev. E* **49**, 751 (1994).
 - [17] D. Sagan and D. Rubin, Linear analysis of coupled lattices, *Phys. Rev. ST Accel. Beams* **2**, 074001 (1999).
 - [18] Y. Papaphilippou and F. Zimmermann, Weak-strong beam-beam simulations for the large hadron collider, *Phys. Rev. ST Accel. Beams* **2**, 104001 (1999).
 - [19] Y. Luo, W. Fischer, N. Abreu, X. Gu, A. Pikin, and G. Robert-Demolaize, Six-dimensional weak-strong simulation of head-on beam-beam compensation in the relativistic heavy ion collider, *Phys. Rev. ST Accel. Beams* **15**, 051004 (2012).
 - [20] M. Bassetti and G. A. Erskine, Closed expression for the electrical field of a two-dimensional Gaussian charge, Technical Report No. CERN-ISR-TH-80-06, 1980.
 - [21] J. Qiang, M. A. Furman, and R. D. Ryne, Parallel simulation of beam-beam interaction in high energy accelerators, Lawrence Berkeley National Laboratory, Berkeley, CA, Technical Report No. LBNL-50786, 2002.
 - [22] M. A. Furman, Beam-beam tune shift and dynamical beta function in PEP-II, Report No. LBL-34957, 1994.